Mon. Not. R. Astron. Soc. **368,** 599–608 (2006) doi:10.1111/j.1365-2966.2006.10154.x

The effect of low-mass substructures on the cusp lensing relation

Andrea V. Macciò★ and Marco Miranda
Institute for Theoretical Physics, University of Zürich, CH-8057 Zürich, Switzerland

Accepted 2006 January 30. Received 2006 January 27; in original form 2005 September 26

ABSTRACT

It has been argued that the flux anomalies detected in gravitationally lensed quasi-stellar objects (QSOs) are evidence for substructures in the foreground lensing haloes. In this paper, we investigate this issue in greater detail, focusing on the cusp relation which corresponds to images of a source located to the cusp of the inner caustic curve. We use numerical simulations combined with a Monte Carlo approach to study the effects of the expected power-law distribution of substructures within Λ cold dark matter (ΛCDM) haloes on the multiple images.

Generally, the high number of anomalous flux ratios in the cusp configurations is unlikely to be explained by 'simple' perturbers (subhaloes) inside the lensing galaxy, modelled by either point masses or extended Navarro, Frenk & White subhaloes. We considered in our analysis a mass range of 10^5–10^7 $M_\odot$ for the subhaloes. We also demonstrate that including the effects of the surrounding mass distribution, such as other galaxies close to the primary lens, does not change the results. We conclude that triple images of lensed QSOs do not show any direct evidence for dark dwarf galaxies such as CDM substructure.

Key words: gravitational lensing – methods: numerical – galaxies: haloes – cosmology: theory – dark matter.

1 INTRODUCTION

Cold dark matter (CDM) simulations predict many more low-mass satellite haloes than are actually observed in the Milky Way (Klypin et al. 1999; Moore et al. 1999). It seems that 10–15 per cent of the mass was left in satellites with perhaps 1–2 per cent at the projected separations of 1–2 Einstein radii (R_e) where we see most lensed images (e.g. Zentner & Bullock 2003; Mao et al. 2004); this is far larger than the observed fraction of 0.01–0.1 per cent in the observed satellites (e.g. Chiba 2002). Solutions to this mismatch were proposed in three broad classes: satellites are present but dark if star formation is prevented (Bullock, Kravtsov & Weinberg 2000), satellites are destroyed due to self-interacting dark matter (Spergel & Steinhardt 2000), or their formation is prevented by changing the power spectrum to something similar to warm dark matter with significantly less power on the relevant mass scales (e.g. Bode, Ostriker & Turok 2001). These hypotheses left the major observational challenge of distinguishing dark satellites from non-existent ones. This became known as the CDM substructure problem.

It has been argued that a possible signature of the presence of dark matter substructures can be found in strong gravitational lensing of quasi-stellar objects (QSOs) (Mao & Schneider 1998; Metcalf & Madau 2001; Chiba 2002; Dalal & Kochanek 2002; Metcalf & Zhao 2002; Kochanek & Dalal 2004). If a distant image source is close to a cusp (from inside) in a caustic curve, three of the images will be clustered together and the sum of their magnifications will be zero (Zakharov 1995), taking the negative parity image to have negative magnification. This relation holds for a wide class of smooth analytic lens models (Keeton, Gaudi & Petters 2003); on the other hand all known observed lensed QSOs violate this relation. This has been explained with the presence of CDM substructures within the lensing galaxy's halo.

However, the discrepancy found in some systems may be due to the microlensed stars rather than to the CDM substructures (Keeton et al. 2003), even if the most peculiar problem is the anomalous flux ratios in radio lenses. Radio sources are essentially unaffected by the interstellar medium (ISM) of the lens galaxy (see, however, Koopmans et al. 2003), true absorption appears to be rare, radio sources generally show little variability and most of the flux should come from regions too large to be affected by microlensing. Therefore, dark matter subhaloes appear to be the most likely explanation.

By using low-resolution simulation of galaxy formation Bradač et al. (2004) claimed that the level of substructures present in simulation produces violations of the cusp relation comparable to those observed. Amara et al. (2006) implanted an idealized model of a galaxy into the centre of a high-resolution galactic halo extracted from the dissipationless *N*-Body simulations to test the effects of substructures on the lensed images. Their findings are contrast to those of Bradač et al. (2004), since they found that the substructures produced in a ΛCDM halo are not abundant enough to account for the observed cusp–caustic violation. The results of Amara et al. (2006) were also confirmed in a recent work by Macciò et al. (2006). In the latter work, in which a fully hydrodynamical

★E-mail: andrea@physik.unizh.ch

simulation of galaxy formation is used, it is shown that the presence of a dissipative component greatly enhances the surviving probability of satellites, expecially close to the centre of the galaxy. Nevertheless, Macciò et al. (2006) also demonstrated that the impact on lensing of subhaloes in the mass range 10^7–$10^{10}\,M_\odot$ is very small. Even with a number of subhaloes about eight higher than the observed one in this mass range, the number of multiple-lensed QSOs that show a violation of the cups relation is less than 24 per cent, in contrast with an observed one of about 60 per cent. This means that if the violation of the cusp relation is due to substructures inside the primary lens, these must have a mass smaller than $10^7\,M_\odot$.

The aim of this work is to study the influence of subhaloes with mass range 10^5–$10^7\,M_\odot$ on the cusp relation violation.

The outline of the paper is the following: first, we briefly summarize the cusp relation, then in Section 3, we present the lensing numerical simulations and our modelling for the primary lens, subhaloes and extrahaloes. Tests for our models and results for three different cusp configurations are presented in Section 4. Section 5 is devoted to a short discussion on the fold relation. A discussion of the results and our conclusions are presented in Section 6. Throughout this paper, the single large halo that is causing the QSO multiple images is referred to as the primary lens. The additional small-scale haloes (inside the host halo) are referred to as subhaloes or substructures. Haloes beyond the virial radius of the primary lens are referred to as extragalactic haloes. We adopt the standard ΛCDM cosmological model with the following parameters $\Omega_m = 0.3$, $\Omega_\Lambda = 0.7$, $\sigma_8 = 0.9$ and $H_0 = 70\,\mathrm{km\,s^{-1}\,Mpc^{-1}}$.

2 THE CUSP RELATION

There are basically three configurations of four-image systems: fold, cusp, and cross (Schneider & Weiss 1992). In this paper, we will mainly concentrate on the cusp configuration that corresponds to a source located close to the cusp of the inner caustic curve. The behaviour of gravitational lens mapping near a cusp was first studied by Blandford & Narayan (1986), Schneider & Weiss (1992), Mao (1992) and Zakharov (1995), who investigated the magnification properties of the cusp images and concluded that the sum of the signed magnification factors of the three merging images approaches zero as the source moves towards the cusp. In other words (e.g. Zakharov 1995) :

$$R_{\rm cusp} = \frac{\mu(A) + \mu(B) + \mu(C)}{|\mu(A)| + |\mu(B)| + |\mu(C)|} \to 0, \quad \text{for } \mu_{\rm tot} \to \infty, \qquad (1)$$

where $\mu_{\rm tot}$ is the unsigned sum of magnifications of all four images, and A, B and C are the triplet of images forming the smallest opening angle (see Fig. 7). By opening angle, we mean the angle measured from the galaxy centre and being spanned by two images of equal parity. The third image lies inside such an angle. This relation is an asymptotic relation and holds when the source approaches the cusp from inside the inner caustic 'astroid'. This can be shown by expanding the lensing map to third order in the angular separation from a cusp (Schneider & Weiss 1992). Small-scale structure on scales smaller than the image separation will cause $R_{\rm cusp}$ to differ from zero fairly independently of the form of the rest of the lens. Indeed, a substructure is more likely to reduce the absolute magnification for negative magnification images (Metcalf & Madau 2001; Schechter & Wambsganss 2002; Keeton et al. 2003) and to increase it for positive parity images.

3 LENSING SIMULATIONS

We use the LENSMODEL package (Keeton 2003a)[1] modelling the main lens galaxy as a singular isothermal ellipsoid (SIE) and the substructures as NFW (Navarro, Frenk & White 1997) haloes. First, using the GRAVLENS task, we find three lens configurations for which the cusp relation is roughly satisfied (Figs 7, 10 and 16).

As a second step, a variable number of substructures is added to the main lens (see Section 3.2 for details on their number density and physical properties). For this new lensing system (main lens plus subhaloes), we compute again positions and fluxes of the images [subhaloes mainly tend to modify fluxes more than positions, see Kochanek, Schneider & Wambsganss (2004) and Section 4.1], obtaining a new value for the cusp relation $R_{\rm cusp}$. This procedure is repeated more than 20 000 times for each of the three studied positions of the source (Figs 7, 10 and 16): this allows us to compute the probability distribution of the $R_{\rm cusp}$ value in presence of subhaloes (i.e. Fig. 8).

3.1 Primary lens

The observed discrepancy in the flux ratios, compared with the expected universal relation from a cusp or fold singularity, suggests that it is an intrinsic difficulty for smooth lens models, not associated with a particular parametrization. For the scope of this paper, it is sufficient to choose just a single smooth lens model for the primary lens. Therefore, we select, as a smooth lens model, an SIE (Kormann, Schneider & Bartelmann 1994) to take advantage of its simplicity. This model has been widely used in lens modelling and successfully reproduces many lens systems (e.g. Keeton, Kochanek & Falco 1998; Chiba 2002; Treu & Koopmans 2004). An isothermal profile for the total mass distribution of elliptical galaxies is well supported by the detailed dynamical studies of local ellipticals (Gerhard et al. 2001), individual lens modelling, and statistics (e.g. Maoz & Rix 1993; Kochanek 1995; Grogin & Narayan 1996).

The ellipsoidal primary lens has a mass equal to $5 \times 10^{11}\,M_\odot$, it is oriented with the major axis along the y-axis in the lens plane and has an ellipticity of 0.33. The redshifts of the lens and the source are fixed to $z_l = 0.3$ and $z_s = 1.71$, respectively, agreement with the typical observed ones (in this case, we use the PG1115+080 data; see Tonry 1998)

3.2 Subhaloes

Since it has been shown that the number density of subhaloes with mass $M > 10^7\,M_\odot$ is not sufficient to explain the observed number of violation in the cusp relation (Amara et al. 2006; Macciò et al. 2006), the aim of this work is to investigate the impact of substructures below this mass threshold that is fixed by the current resolution limits of the numerical simulations.

We would like to emphasize that we are using only one lensing plane, this means that we will consider only effects due to substructures being at the same redshift of the main lens [see Chen, Kravtsov & Keeton (2003) and Metcalf (2005) for an estimation of the effects of haloes along the line of sight]. In order to evaluate the number density substructures in the mass range 10^5–$10^7\,M_\odot$, we have made some extrapolations based on the results from the high-resolution N-body simulations. The mass function of subhaloes inside the virial

[1] The software is publicly available via the web site: http://cfa-www.harvard.edu/castles.

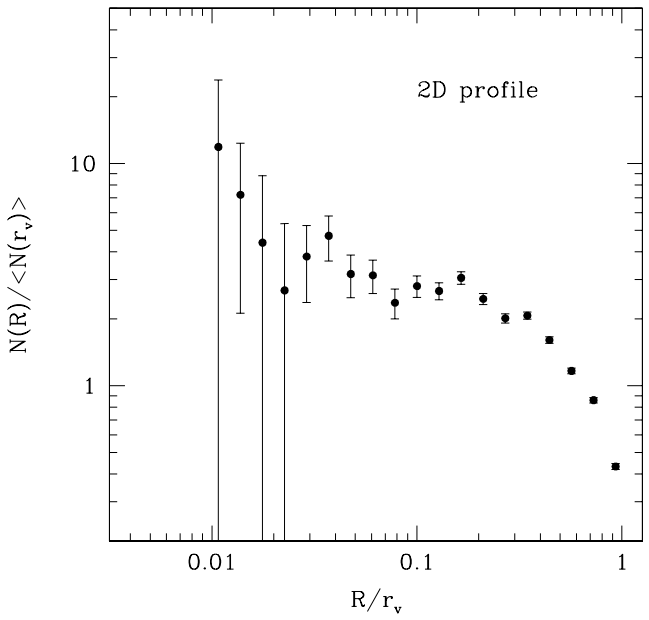

Figure 1. Two-dimensional radial number density of subhaloes in units of the average number density inside the virial radius. Result obtained averaging the four high-resolution galaxies presented in DMS04, using three different projections for each galaxy.

radius of a halo is close to a power law (Diemand, Moore & Stadel 2004, DMS04 hereafter; Gao et al. 2004; Reed et al. 2005):

$$N(>m) \propto m^{-\beta}, \tag{2}$$

with a slope $\beta \approx 1$, so that we expect to have a factor of $\approx$100 more subhaloes inside the viral radius if we move our mass threshold from 10^7 to $10^5\,\mathrm{M}_\odot$.

As said in the previous section, such small haloes will affect the $R_{\rm cusp}$ relation only if their distance from the images is of the same order or smaller than the distance between the images themselves. Therefore, we need an estimation of the number of haloes inside a small area surrounding the images. This number will also depend on the distance of our area from the centre, due to the fact that the number density of haloes increases while approaching the centre of the main halo (primary lens) as clearly shown in Fig. 1, which is based on the numerical simulations of four galaxy-sized haloes (DMS04).

Consequently, the number of subhaloes with a mass greater than m inside an area A at a distance R from the centre of the galaxy is

$$N_A(>m, R) = \frac{\langle N_{r_v}(>m_0)\rangle (m_0/m) N(R) A}{\pi r_{\rm v}^2}, \tag{3}$$

where $\langle N_{r_v}(>m_0)\rangle$ is the average number density of subhaloes with $m > m_0$ (being m_0 an arbitrary mass value) inside the virial radius r_v and $N(R)$ is the radial 2D number density of satellites at a projected distance R from the centre in units of $\langle N_{r_v}(>m_0)\rangle$ (see Fig. 1). These last two quantities can be obtained directly from the N-body simulations. In the following, we will use results from DMS04 (table 1 of their paper, simulations G0–G3). Macciò et al. (2006) have shown that the presence of baryons inside subhaloes enhance the probability to find haloes close to the centre of the galaxy with respect to results from the dissipationless simulations. This is true for satellites with $m > 5 \times 10^7\,\mathrm{M}_\odot$, which are massive enough to retain baryons inside their potential well and then form stars. Since, we do not expect such effect for the mass scales involved in this work ($\approx 10^5$–$10^6\,\mathrm{M}_\odot$), we can use pure N-body simulation as starting point for our analysis.

Since, the typical separation between images in the lensed QSOs is roughly a few arcsec, we fix $R \approx 1$ arcsec and $A = 6$ arcsec^2 (A_6 hereafter). We remind that at a redshift of $z_l = 0.3$, 1 arcsec corresponds to 4.55 kpc for the cosmological model adopted in this paper. Using equation (3) and adopting a mass threshold for substructures of $m = 5 \times 10^5\,\mathrm{M}_\odot$, the number of subhaloes inside A ranges from four to 12 [depending on the uncertainties on $N(R)$, see Fig. 1]. For two $10^7\,\mathrm{M}_\odot$ haloes, the surface mass density within the selected area A is $0.69\,h^{-2}\,\mathrm{M}_\odot\,\mathrm{pc}^{-2}$, this means a fraction of $\approx 10^{-3}$ of the total dark matter surface density in substructures, in good agreement with the results of Mao et al. (2004).

For each lensing configuration analysed in this work, we added a random number of substructures between four and 12 to the primary lens with a random mass generated according to equation (2) in the range 5×10^5–$10^7\,\mathrm{M}_\odot$. These subhaloes are then placed following the 2D density profile inside the area A_6 that encloses the three images [cf. the (blue) square in Fig. 7]. We have modelled our subhaloes with an NFW density profile; for the $\approx 10^6\,\mathrm{M}_\odot$ subhaloes relevant for lensing substructure studied in this work, the NFW profile inferred from the N-body simulation is the most natural choice, because on these mass scales, the effect of baryons (that are able to modify the slope of the density profile for greater masses, see Macciò et al. 2006) is very tiny because the potential well of these haloes is not deep enough to retain them expecially in presence of a ionizing background. We have adopted different concentration parameters (see Section 4.1) to mimic the scatter present in the mass–concentration relation (Bullock et al. 2001).

3.3 Extrahaloes

Lensing galaxies are not isolated object, since they usually belong to group of galaxies (Keeton, Christlein & Zabludoff 2000). Moreover, each galaxy has its own satellite galaxies with masses in the range 10^9–$10^{11}\,\mathrm{M}_\odot$. Consequently, we have modelled the presence of these *extrahaloes* in the same way as the *innerhaloes*. In this work, we call substructures or innerhaloes, haloes with $M < 10^7\,\mathrm{M}_\odot$ that are close to the image position; we reserve the term extrahaloes for haloes with $M > 10^9\,\mathrm{M}_\odot$. We do not consider extrahaloes that appear to lie inside the primary lens close to the image positions because of projection effects (i.e. Oguri 2005).

We considered three different categories of extrahaloes: (i) haloes with mass $10^9 < M < 10^{10}\,\mathrm{M}_\odot$ and with a projected distance r between 60 and 200 kpc, these represent the satellite galaxy of the primary lens (the expected number for these haloes can be estimated again form the N-body simulation and it is roughly six to eight); (ii) haloes with mass $10^{11} < M < 10^{12}\,\mathrm{M}_\odot$ and distance $300 < r < 700$ kpc in order to mimic the presence of companion galaxies and (iii) haloes with mass $10^{12} < M < 5 \times 10^{13}\,\mathrm{M}_\odot$ and distance $700 < r < 1200$ kpc to take into account the possible presence of a nearby cluster of galaxies.

The number of extrahaloes has been fixed between two to eight and two to four for the (ii) and (iii) case, respectively, as suggested by observations/simulations (Metcalf 2005; Amara et al. 2006). While the extrahaloes in case (i) are placed in a circularly symmetric way around the centre of the galaxy, the position of groups and clusters of galaxies must be modelled in an asymmetric way. Therefore, we placed them only in the quadrant with positive coordinates in the lens plane (being the lens in [0 : 0]). We used the SIE as lens model for extrahaloes to take into account the presence of baryons inside them and we have generated 20 000 different configurations.

4 RESULTS

In this section, we present results of our Monte Carlo simulations. We have analysed three cusp configurations: Config1 (Fig. 7), Config2 (Fig. 10) and Config3 (Fig. 16). They mainly differ for the value of $R_{\rm cusp}$ in the unperturbed case that grows from 0.01 for Config1 to 0.243 for Config3, due to a different position of the source inside the inner caustic curve.

4.1 Testing our model

Before proceeding further in our analysis, we present some tests on the parameter adopted in our lensing simulation. The presence of substructures acts both on positions and fluxes of the images. When a substructure is added the GRAVLENS code adjusts the positions and fluxes of the images by minimizing the χ^2 between the old (unperturbed) and new (perturbed) positions/fluxes. The value of χ^2 depends on the error that we assign to the unperturbed positions and fluxes (usually these are the observational errors); this means that if the error on positions is smaller than the error on fluxes, the code will change the latter ones more than moving the images to obtain a lower value for χ^2.

Therefore in principle, the value of the perturbed $R_{\rm cusp}$ is influenced by the error assigned to the position of the images. In Fig. 2, we clearly show that this effect is very small even for a big variation of the image position errors. This plot illustrates the probability distribution for $R_{\rm cusp}$ (obtained using 20 000 realizations), when four substructures are added to the primary lens: the solid line is for an error on positions of $\epsilon_1 = 10^{-2}$ arcsec (≈5 per cent) and the dashed one for $\epsilon_2 = 10^3$ arcsec (i.e. the code has complete freedom in moving the images). The two distributions of the $R_{\rm cusp}$ values are very similar, and these also confirm findings of other authors: the influence of the substructures on the image positions is less strong than the one on fluxes (Kochanek 2004). We will adopt 10^{-2} arcsec for the error on positions for all our simulations.

A correct determination of the subhaloes properties (see Section 3.2) is a key ingredient in computing the $R_{\rm cusp}$ value: Fig. 3 shows the influence of the number density and mass range of substructures on the $R_{\rm cusp}$ relation. Both changing the area in which subhaloes are distributed (keeping fixed their number: left-hand panel) or their mass range (right-hand panel) leads to complete different results.

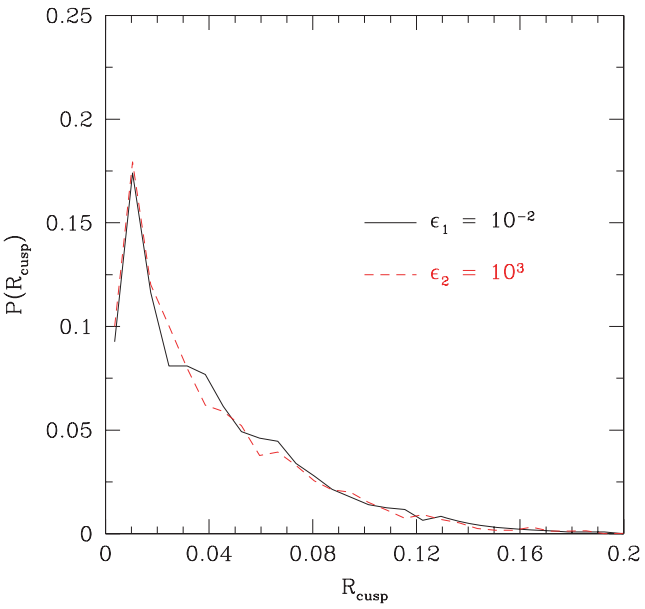

Figure 2. Probability distribution of $R_{\rm cusp}$ values for the two substructures inside A_3 for different position errors.

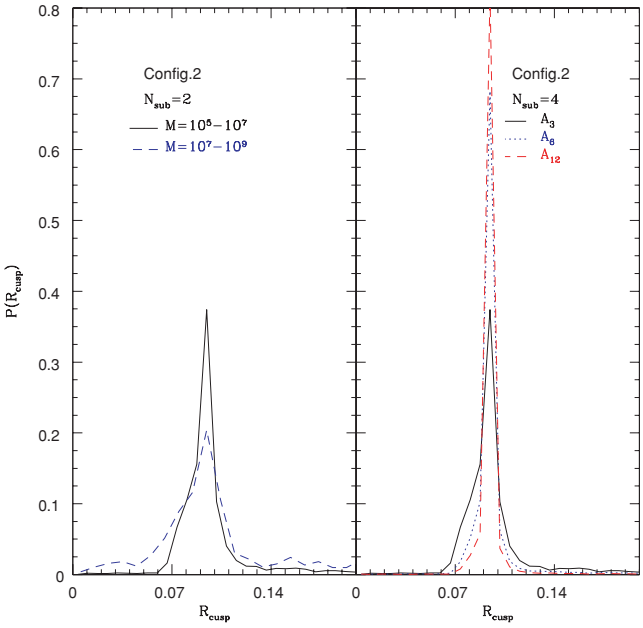

Figure 3. Probability distribution of $R_{\rm cusp}$ with four substructures. Left-hand panel: influence of the substructure mass. Right-hand panel: effects of the projected number density.

As a second step, we have tested if the subhaloes that live outside the small area (A) surrounding the images can substantially modify the $R_{\rm cusp}$ relation. For this purpose, we have defined three different areas for substructures for Config2: $A_3 = [-1.5 : 1.5] \times [1 : 2]$, $A_6 = [-1.5 : 1.5] \times [0 : 2]$ and $A_{12} = [-1.75 : 1.75] \times [-1.25 : 2.25]$. The last one ($A_{12}$) is big enough to cover all the image positions. Changing the size of the area and his position with respect to the centre of the lens, the number of substructures changes according to equation (3). The number of subhaloes inside the three areas is four, nine and 19, respectively. Fig. 4 shows our results. The $R_{\rm cusp}$ probability distribution is weakly affected by the size of the area. This indicates that the subhaloes close to the image positions are the ones responsible for the $R_{\rm cusp}$ relation modification.

Fig. 5 shows results for Config2 (Fig. 10) of the $R_{\rm cusp}$ probability distribution for the three subhaloes with mass $5 \times 10^5 < m < 10^7\,{\rm M}_\odot$ inside A_3 (solid line), and for the eight subhaloes with $10^7 < m < 10^9\,{\rm M}_\odot$ inside an area of 57 arcsec^2 ($[-5 : 5] \times [0 : 6]$ with the exclusion of A_3). For this second population of substructures, both the number density and the masses are overestimated by a large fraction. Nevertheless, its effect on the cusp relation is very small and the $R_{\rm cusp}$ probability distribution is close to a delta function centred on the unperturbed value.

Modelling our subhaloes as NFW structures, we have one more free parameter: the concentration. It is well known that the concentration correlates with the mass of the halo, even if a consistent scatter is present in this relation. Extrapolating results from Bullock et al. (2001), the mean concentration in our mass range is around 33. In order to test the influence of the concentration of our subhaloes in modifying the $R_{\rm cusp}$ relation, we repeated our analysis keeping fix mass and position of the subhaloes and varying their concentrations. Results are shown in Fig. 6. As expected, denser haloes have

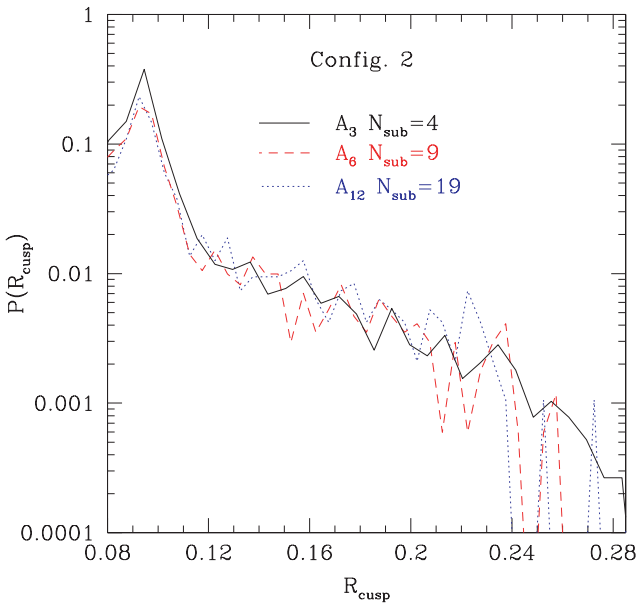

Figure 4. Probability distribution of $R_{\rm cusp}$ for substructures distributed on different areas.

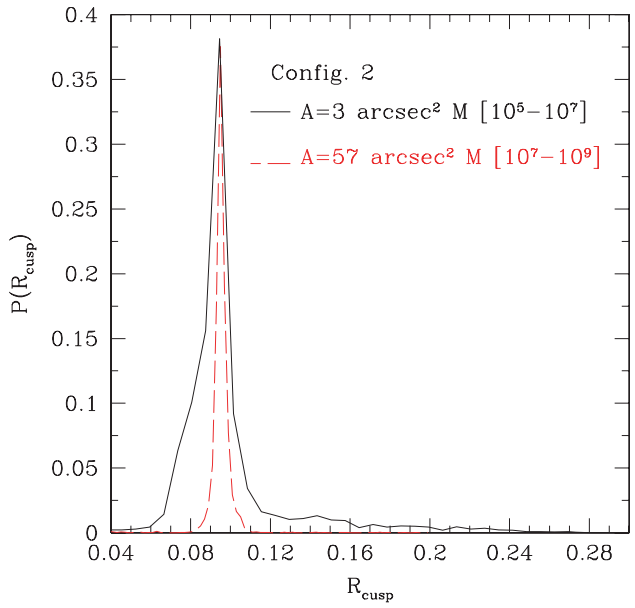

Figure 5. Effects on the $R_{\rm cusp}$ relation of the substructures inside a small area (A_3) surrounding the images (solid line) and in a larger area $[-5:5]\times[0:6]$ (57 arcsec) outside A_3 (dashed line). In the first case, the substructures are in the mass range $[5\times10^5{:}10^7\,{\rm M}_\odot]$ and $[10^7:10^9\,{\rm M}_\odot]$ in the second one.

a stronger impact on the $R_{\rm cusp}$ relation. We have also considered two other mass profiles for the subhaloes: singular isothermal sphere (SIS) and point-like approximation. The first one, less favoured by simulations, can be seen as an upper limit for the NFW profile, due to the fact that its inner slope for the density profile is proportional to r^{-2}. For this kind of subhalo model the $R_{\rm cusp}$ probability is just slightly above the ones for NFW haloes with $c=35$, so we do not expect a big change in our results using SIS instead of NFW subhaloes. On the other hand, the point-mass approximation leads to an underestimate of the effect of subhaloes on $R_{\rm cusp}$ since for a

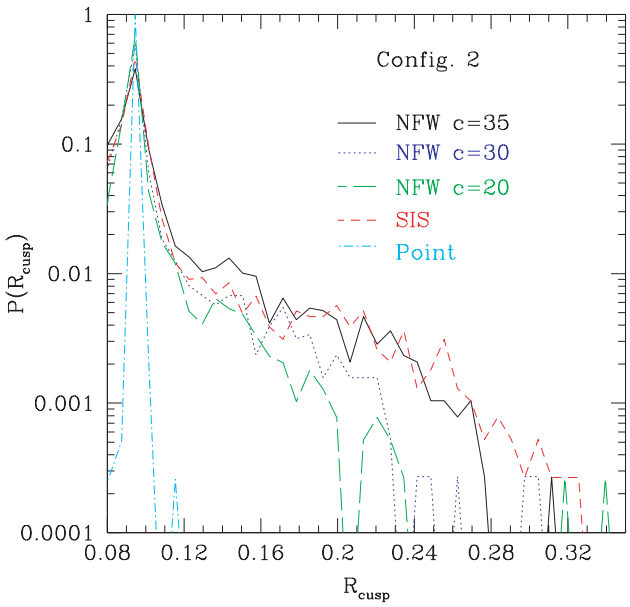

Figure 6. $R_{\rm cusp}$ distribution probability for different subhaloes mass profiles: NFW profile with different concentration values, SIS profile and point-like approximation.

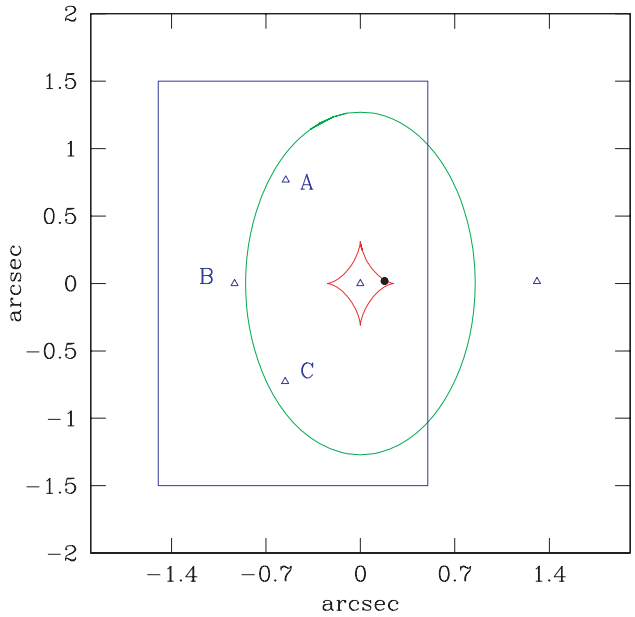

Figure 7. Unperturbed lens configuration: Config1 ($R=0.01$).

fixed mass a point-like object has a smaller Einstein radius than an NFW halo (Keeton 2003b). In the following, we have adopted a concentration parameter of 35 for our subhaloes in order to try to maximize their effect on the $R_{\rm cusp}$ relation.

4.2 Configuration 1

In the first configuration analysed (Config1 hereafter), the source is close to the right cusp of the inner caustic curve (see Fig. 7) and the unperturbed $R_{\rm cusp}$ value is 0.01. The critical and caustic curves refer to the unperturbed case but they are not different from perturbed ones at the level of resolution.

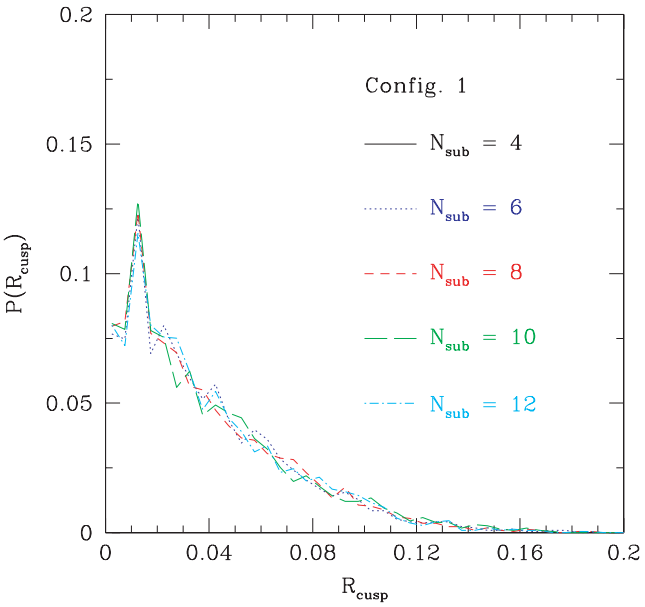

Figure 8. Probability distribution of R-variation for a different number of substructures inside A_6.

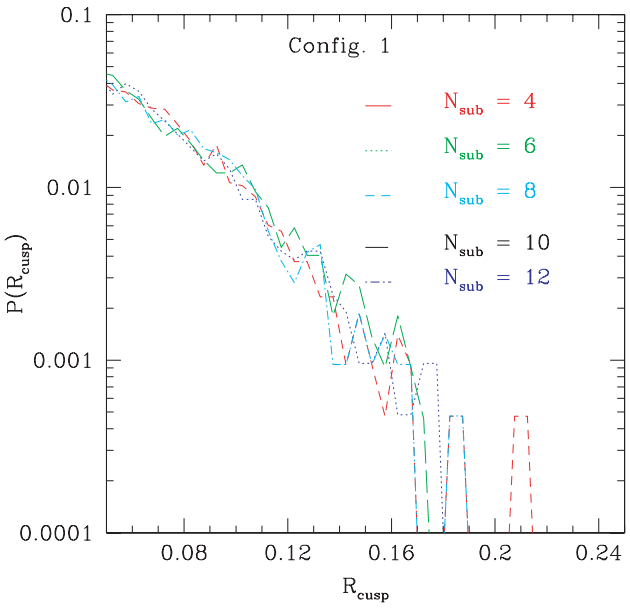

Figure 9. Same as Fig. 8 with logarithmic scale for the y-axis.

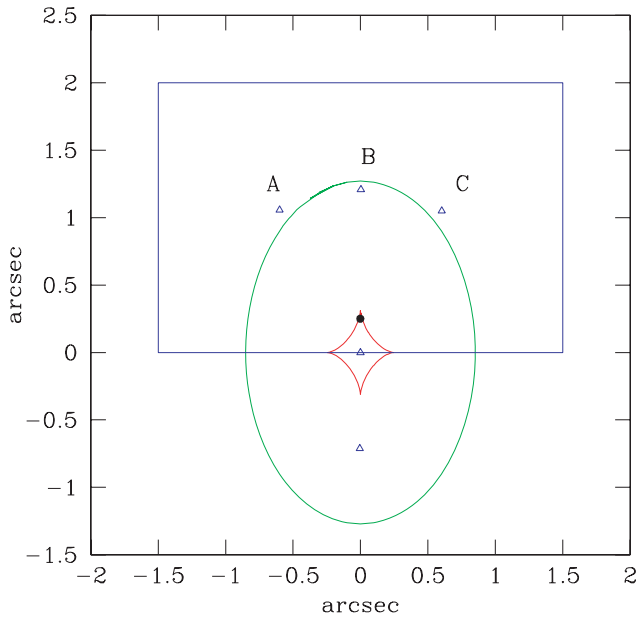

Figure 10. Second unperturbed lens configuration: Config2 ($R = 0.09$).

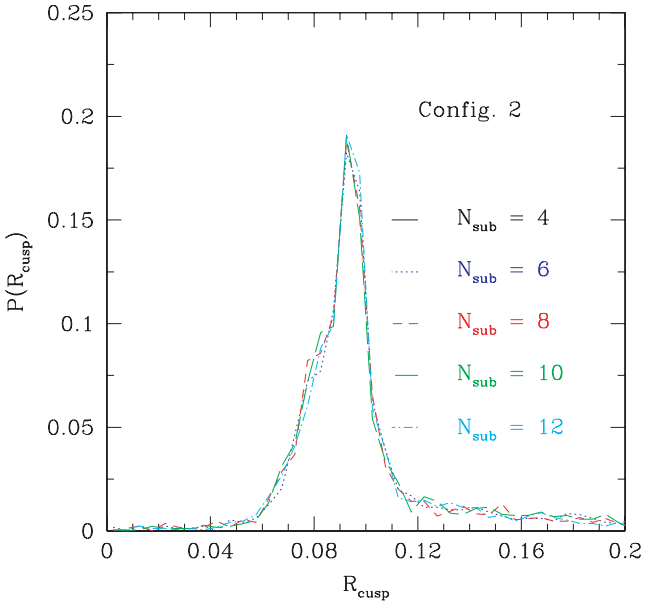

Figure 11. Probability distribution of R-variation for Config 2, for a different number of substructures inside A_6.

For this configuration, we have generated 20 000 different lensing systems that include substructures according to equation (3). In Fig. 8, the probability distribution for $R_{\rm cusp}$ for different numbers of substructures is shown. The maximum of the probability is obtained for the unperturbed value (0.01) and the tail of the distribution extends to $R_{\rm cusp} = 0.12$ but for a very low number of configurations (less than 1.0 per cent). Fig. 9 shows in a logarithmic plot the tail of the distribution presented in Fig. 8: it is possible to note that an increase of the total number of substructures (from four to six) does not substantially change the value of $R_{\rm cusp}$.

From Fig. 8, one sees that in the 10 per cent of the configurations the final value of $R_{\rm cusp}$ is even less than the unperturbed value, and it is closer to the theoretical expectation of $R_{\rm cusp} = 0$ (see Section 4.3 on the second configuration for more details).

4.3 Configuration 2

In this configuration (Config2 hereafter), the source is close to the upper cusp of the inner caustic curve (see Fig. 10) with an unperturbed value of $R_{\rm cusp} = 0.09$.

Fig. 11 is analogous to Fig. 8 for Config2 and Fig. 12 shows the tail of the distribution for large values of $R_{\rm cusp}$. Even in this case, the maximum of the probability distribution is centred on the unperturbed value. Here, the distribution of the values of $R_{\rm cusp}$ is more symmetric than for Config1 and it is more evident that the

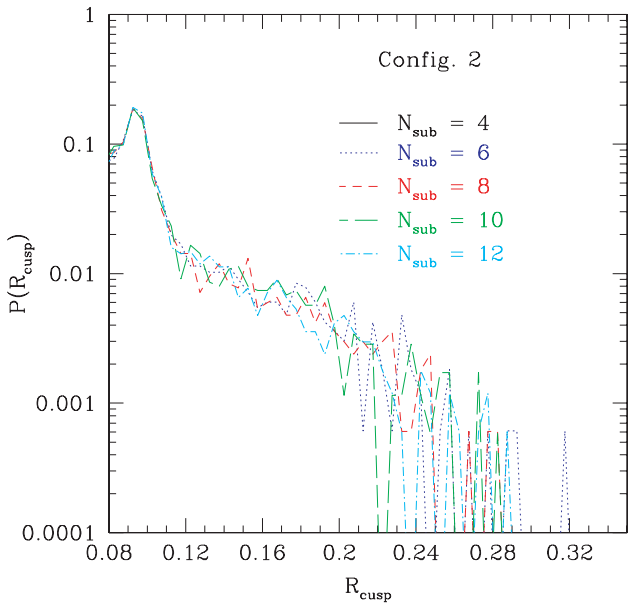

Figure 12. Same as Fig. 11 with logarithmic scale for the *y*-axis.

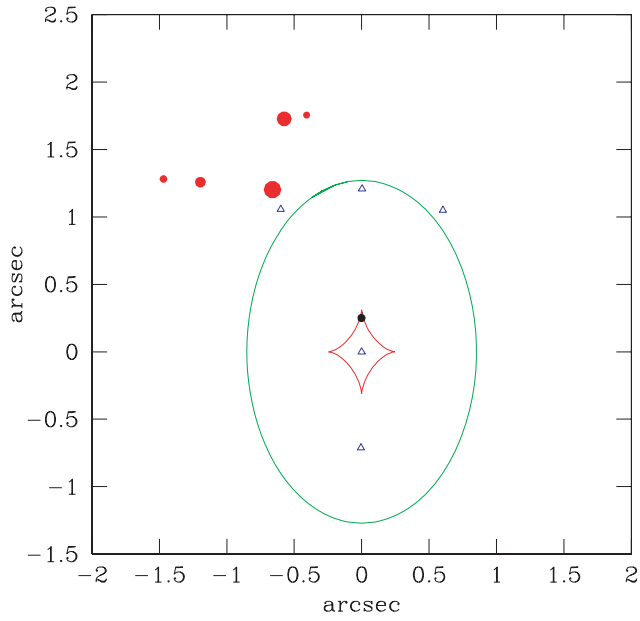

Figure 13. One perturbed configuration where $R_{\rm cusp}$ is less than the unperturbed value (0.091 versus 0.07). The solid circles show the position of the subhaloes, the point size is proportional to their mass.

effect of substructures not only increase the value of the cusp ratio but can also reduce it.

To better illustrate this effect, we have isolated one of the configurations in which we find a reduction of $R_{\rm cusp}$ (Fig. 13). When the distribution of subhaloes is non-symmetric with respect to the triplets of images and one of the perturbers is close to one of the external images the latter image results to be more magnified than the others. In the unperturbed configuration: $|\mu(B)| > \mu(A) + \mu(C)$ and this causes $R_{\rm cusp} \neq 0$. On the other hand, if the perturbers increase $\mu(A)$ without changing considerably the magnification of the other images, this will enhance the sum $\mu(A) + \mu(C)$ pushing it closer to $\mu(B)$, giving a smaller $R_{\rm cusp}$ (0.07 in the case of Fig. 13).

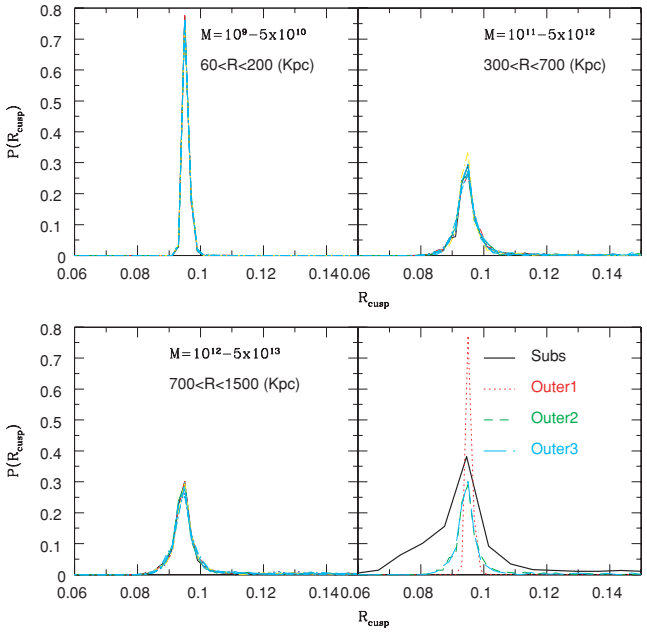

Figure 14. Probability distribution of *R*-variation considering extrahaloes with different masses and distances from the primary lens (Config2). Bottom right-hand panel: comparison between the effects of extrahaloes and subhaloes.

Fig. 14 shows the effects of extrahaloes on the $R_{\rm cusp}$ value for Config2. For all the three extrahaloes mass ranges considered, the modifications in the cusp relation are very small and the value of $R_{\rm cusp}$ is not very sensitive to the total number of extrahaloes we generated (results for different number of subhaloes are shown by different curves, which are almost overlapping in the various panels).

For this configuration, we have performed one more test: we have modified by hand the fluxes of the three images in order to obtain an high value of $R_{\rm cusp}$ (>0.37). Then, we used the GRAVLENS software to find positions and masses of two subhaloes (with masses $5 \times 10^5 < M < 5 \times 10^6$ $M_\odot$) with the constraint of simultaneously reproducing positions and fluxes of our modified images. We have found two configurations for subhaloes that are shown in Fig. 15. In the first case (solid squares), the mass of the substructures is roughly the same ($\approx 2.0 \times 10^6$), they are close to the external images with a distance of 0.08 arcsec and the perturbed value of $R_{\rm cusp}$ is 0.387. In the second case (open circles), the mass of the subhalo close to the central image is 1.6×10^5 $M_\odot$ with a distance of 0.06 arcsec, while 7.8×10^5 $M_\odot$ is the mass of the second one that is far away from the central image, for a perturbed value of $R_{\rm cusp}$ equal to 0.372.

The aim of this test is to show that there is nearly always the possibility to explain an anomalous flux ratio using subhaloes, but their positions and masses must be tuned in a very precise way (i.e. distances between images and subhaloes must be less than 0.08 arcsec). Most important, our Monte Carlo simulations show that the probability of obtaining such a fine tuning is very low. As a consequence, we conclude that an explanation for the high number of observed anomalous flux ratios in the lensed QSOs based on the presence of subhaloes in the mass range we have tested is very unlikely.

4.4 Configuration 3

In the last cusp configuration analysed (Config3), the $R_{\rm cusp}$ relation is not completely satisfied even in the unperturbed case ($R_{\rm cusp}$ =

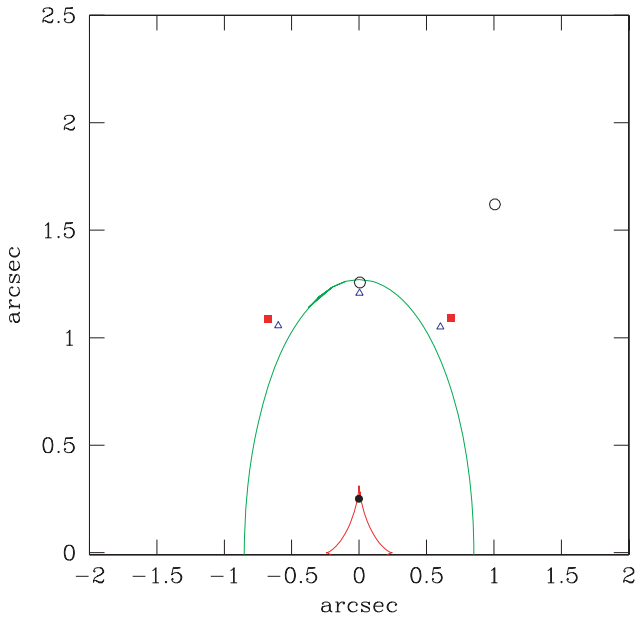

Figure 15. Two subhaloes configurations with high $R_{\rm cusp}$ value. The first one (indicated by solid squares) gives $R_{\rm cusp} = 0.387$. The second one (indicated by open circles) gives $R_{\rm cusp} = 0.274$. In both cases, $M_{\rm sub} \approx 10^6$.

0.243, see Fig. 16). Fig. 17 shows the $R_{\rm cusp}$ probability distribution for Config2 and Config3 normalized to the unperturbed value. There are no appreciable differences between the two configurations. The probability distributions have almost the same width and the same maximum value (≈0.35) and both are centred on the respective unperturbed value. This means that the ability of substructures to modify the $R_{\rm cusp}$ relation is nearly independent of the original value of the cusp ratio.

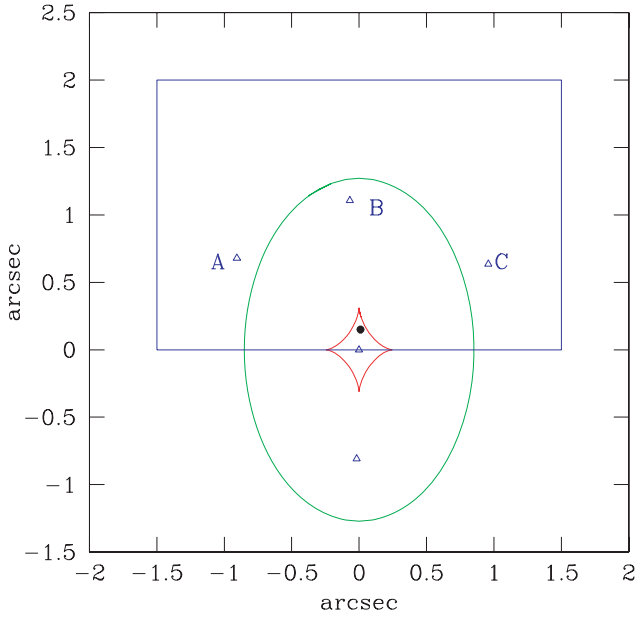

Figure 16. Third unperturbed lens configuration: Config3 ($R = 0.243$).

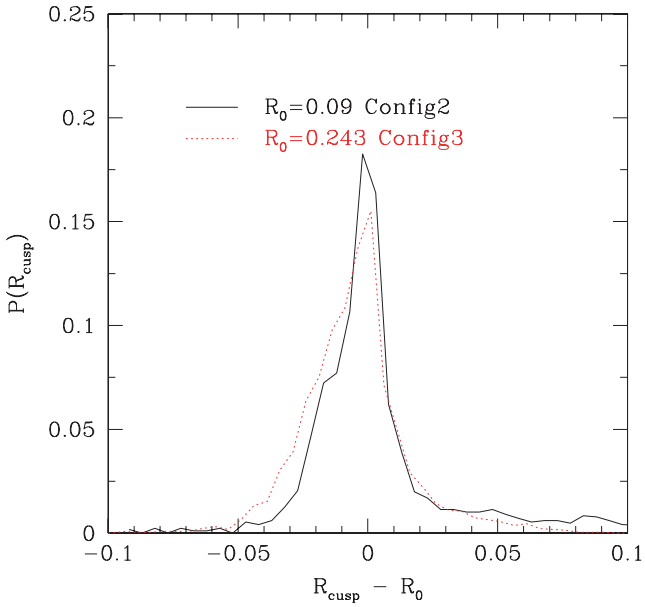

Figure 17. Probability distribution for the four subhaloes within A_6 for Config2 and Config3.

5 FOLD RELATION

For sake of completeness, we have also considered a fold case similar to the configuration of the well-known system PG1115 (Impey et al. 1998). In this case, we define the fold relation as the ratio between the magnification of the closest pair on opposite sides of the critical curve (cf. Fig. 18):

$$R_{\rm fold} = \frac{\mu(A_1)}{\mu(A_2)} = 1. \quad (4)$$

By applying our procedure to this test fold case, we found that it is easier to modify the value of the unperturbed $R_{\rm fold}$ with respect to the one of $R_{\rm cusp}$, as clearly shown in Fig. 19. In our computational procedure, the position of the source can be changed by the GRAVLENS code, in order to minimize the χ^2 of the lens configuration. While this does not affect the $R_{\rm cusp}$ relation, it can be important in the fold case: as pointed out by Keeton, Gaudi & Petters (2005), the degree to which $R_{\rm fold}$ can differ from one for realistic smooth lenses depends, in addition to the angular structure of the lens potential, not only on the distance of the source from the caustic but also on its location along the caustic itself. So the values we got for $R_{\rm fold}$ are due to both the effects of subhaloes and the shift along the caustics of the source.

Thus, it is not possible to conclude from $R_{\rm fold}$ alone that whether the observed flux ratios are anomalous or not.

6 DISCUSSION AND CONCLUSIONS

Quasars that are being gravitationally lensed into multiple images have recently been used to place limits on the surface density of the CDM subhaloes (Mao & Schneider 1998; Metcalf & Madau 2001; Chiba 2002; Dalal & Kochanek 2002; Metcalf & Zhao 2002; Chen et al. 2003; Bradač et al. 2004; Mao et al. 2004). Small mass clumps that happen to lie near the images affect the observed magnification ratios. The question arises as to whether these observations are compatible with distortions expected to occur from dark matter substructures and satellite galaxies within the ΛCDM model. Recent results based on the numerical N-body (Amara et al. 2006; Rozo

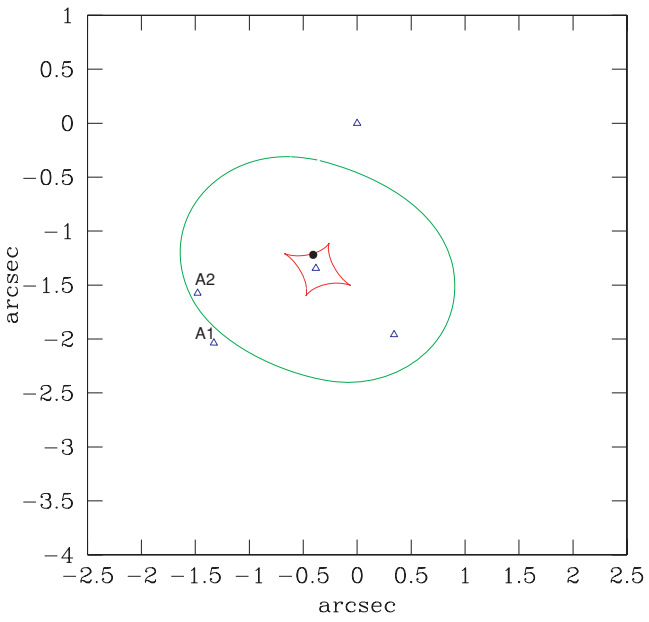

Figure 18. Unperturbed fold lens configuration (similar to PG1115, $R_{\rm fold} = 0.92$).

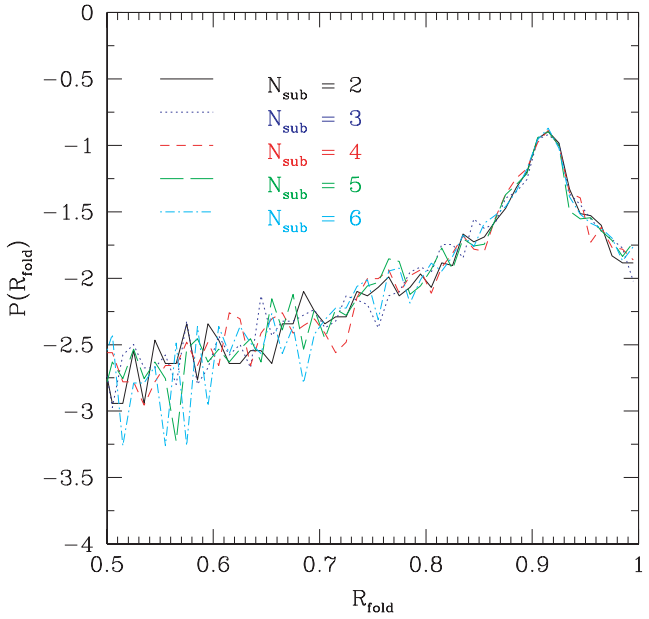

Figure 19. Probability distribution of $R_{\rm fold}$ for a different number of substructures within an area of 3 arcsec^2 ($5 \times 10^5 < M_{\rm sub} < 10^7$ M$_\odot$).

et al. 2006) and hydro simulations (Macciò et al. 2006) have shown that it is hard to reconcile the observed high number of cups relation violation with the total amount of substructures predicted by the ΛCDM model. These studies were limited by the present achievable numerical resolution that permits to resolve the dark matter haloes down to masses $\approx 10^7$ M$_\odot$.

In this work, we have quantified the effects of smaller mass clumps (10^5–10^7 M$_\odot$) on the observed violation of the $R_{\rm cusp}$ relation. We employed results from the N-body simulations to estimate the expected number of subhaloes in this low-mass range. Due to the small mass of the perturbers, we have restricted our analysis only to those close (in 2D) to the positions of the images. For the mass range inspected in this work and for the typical distance between images (few arcsecs), this leads to a number of perturbers $\approx$6. All the subhaloes are modelled as NFW spheres and we have generated more than 10^5 different lensing configurations, varying masses, positions and number of subhaloes.

The main finding of our work is that on a statistical basis this class of perturbers is not able to modify consistently the unperturbed $R_{\rm cusp}$ relation. Values of $R_{\rm cusp}$ in the observed range ($\approx$0.25) are obtained in only less than 1 per cent of the analysed systems. The ability of subhaloes in modifying the unperturbed value of $R_{\rm cusp}$ is found to be independent from the value of $R_{\rm cusp}$ itself.

These results are not in contradiction with the ones in the literature (Keeton et al. 2003; and more recently Miranda & Jetzer 2005, and references therein). As shown in Fig. 15, it is possible to use subhaloes in the mass range 10^5–10^7 M$_\odot$ to obtain high values of $R_{\rm cusp}$ case by case, but a tight *fine tuning* between the location of the images and masses/positions of the perturbers is needed .

In addition, we have also considered the impact of massive haloes placed outside the primary lens (from groups of galaxies to a close cluster) by modelling them in the same way of the subhaloes. Our simulations show, as expected, that their contribution in modifying the $R_{\rm cusp}$ relation is tiny and almost negligible with respect to the effect of the subhaloes.

Results from this work together with results from the numerical simulations seem to be in disagreement with the standard picture which explains the anomalous flux ratio by means of dark matter satellites. Interestingly, while on dwarf galaxy scale there is an excess of dark matter subhaloes with respect to visible satellites, we have shown that the predicted level of substructures on smaller scales is not sufficient to explain the observed level of violation in the cusp relation.

Possible solutions to this problem can reside in microlensing for some of the lensing systems observed in the optical band (Metcalf 2005; Keeton et al. 2006), or in the presence of haloes lying along the line of sight between the lens and the observer (Chen et al. 2003; Metcalf 2005), although the total effect of this kind of perturbers is not yet clear.

ACKNOWLEDGMENTS

We thank Chuck Keeton for making available the GRAVLENS software and for his comments on an early version of this work. We also thank J. Diemand for making available his N-body simulations and M. Bartelmann, Ph. Jetzer and R. Piffaretti for useful discussions. An anonymous referee is also thanked for his suggestions that improved the presentation of this work. Marco Miranda was partially supported by the Swiss National Science Foundation.

REFERENCES

Amara A., Metcalf R. B., Cox T. J., Ostriker J. P., 2006, MNRAS, in press (astro-ph/0411587)
Blandford R., Narayan R., 1986, ApJ, 310, 568
Bode P., Ostriker J. P., Turok N., 2001, ApJ, 556, 93
Bradač M., Schneider P., Lombardi M., Steinmetz M., Koopmans L. V. E., Navarro J. F., 2004, A&A, 423, 797
Bullock J. S., Kravtsov A. V., Weinberg D. H., 2000, ApJ, 539, 517
Bullock J. S., Kolatt T. S., Sigad Y., Somerville R. S., Kravtsov A. V., Klypin A. A., Primack J. R., Dekel A., 2001, MNRAS, 321, 559
Chen J., Kravtsov A. V., Keeton C. R., 2003, ApJ, 592, 24
Chiba M., 2002, ApJ, 565, 17
Dalal N., Kochanek C. S., 2002, ApJ, 572, 25

Diemand J., Moore B., Stadel J., 2004, MNRAS, 352, 535 (DMS04)
Gao L., De Lucia G., White S. D. M., Jenkins A., 2004, MNRAS, 352, L1
Gerhard O., Kronawitter A., Saglia R. P., Bender R., 2001, AJ, 121, 1936
Ghigna S., Moore B., Governato F., Lake G., Quinn T., Stadel J., 2000, ApJ, 544, 616
Grogin N. A., Narayan R., 1996, ApJ, 464, 92
Impey C. D., Falco E. E., Kochanek C. S., Lehár J., McLeod B. A., Rix H.-W., Peng C. Y., Keeton C. R., 1998, ApJ, 509, 551
Keeton C., 2003a, in Proc. ESO Workshop, The Mass of Galaxies at Low and High Redshift, p. 187 (astro-ph/0112350)
Keeton C. R., 2003b, ApJ, 584, 664
Keeton C. R., Kochanek C. S., Falco E. E., 1998, ApJ, 509, 561
Keeton C. R., Christlein D., Zabludoff A. I., 2000, ApJ, 545, 129
Keeton C. R., Gaudi B. S., Petters A. O., 2003, ApJ, 598, 138
Keeton C. R., Gaudi B. S., Petters A. O., 2005, ApJ, 635, 35
Keeton C. R., Burles S., Schechter P. L., Wambsganss J., 2006, ApJ, 639, 1
Klypin A., Kravtsov A. V., Valenzuela O., Prada F., 1999, ApJ, 522, 82
Kochanek C. S., 1995, ApJ, 453, 545
Kochanek C. S., Dalal N., 2004, ApJ, 610, 69
Kochanek C. S., Schneider P., Wambsganss J., 2004, in Meylan G., Jetzer P., North P., eds, Proceedings of the 33rd Saas-Fee Advanced Course, Part 2 of Gravitational Lensing: Strong, Weak & Micro. Springer-Verlag, Berlin, preprint (astro-ph/0407232)
Koopmans L. V. E. et al., 2003, ApJ, 595, 712
Kormann R., Schneider P., Bartelmann M., 1994, A&A, 284, 285
Macciò A. V., Moore B., Stadel J., Diemand J., 2006, MNRAS, 366, 1529
Mao S., 1992, ApJ, 389, 63
Mao S., Schneider P., 1998, MNRAS, 295, 587
Mao S., Jing Y., Ostriker J. P., Weller J., 2004, ApJ, 604, L5
Maoz D., Rix H., 1993, ApJ, 416, 425
Metcalf R. B., 2002, ApJ, 580, 696
Metcalf R. B., 2005, ApJ, 629, 673
Metcalf R. B., Madau P., 2001, ApJ, 563, 9
Metcalf R. B., Zhao H., 2002, ApJ, 567, L5
Miranda M., Jetzer P., 2005, MNRAS, submitted
Moore B., Ghigna S., Governato F., Lake G., Quinn T., Stadel J., Tozzi P., 1999, ApJ, 524, L19
Navarro J. F., Frenk C. S., White S. D. M., 1996, ApJ, 462, 563 (NFW)
Oguri M., 2005, MNRAS, 361, L38
Reed D., Governato F., Quinn T., Gardner J., Stadel J., Lake G., 2005, MNRAS, 359, 1537
Rozo E., Zentner A. R., Bertone G., Chen J., 2006, ApJ, 639, 573
Schechter P. L., Wambsganss J., 2002, ApJ, 580, 685
Schneider P., Weiss A., 1992, A&A, 260, 1
Spergel D. N., Steinhardt P. J., 2000, Phys. Rev. Lett., 84, 3760
Tonry J. L., 1998, AJ, 115, 1
Treu T., Koopmans L. V. E., 2004, ApJ, 611, 739
Zakharov A. F., 1995, A&A, 293, 1
Zentner A. R., Bullock J. S., 2003, ApJ, 598, 49

This paper has been typeset from a TEX/LATEX file prepared by the author.